Density limit in discharges with high internal inductance on JT-60U

journal or publication title	Nuclear Fusion
volume	Vol.47
page range	pp.1418-1424
year	2007-10-01
URL	http://hdl.handle.net/10655/1312

doi: 10.1088/0029-5515/47/11/003

Density Limit in Discharges with High Internal Inductance on JT-60U

H.Yamada 1,2), H.Takenaga 3), T.Suzuki 3), T.Fujita 3), T.Takizuka 3), Y.Kamada 3), N.Asakura 3), T.Tuda 3), M.Takechi 3), G.Matsunaga 3), Y.Miura 3)

1) National Institute for Fusion Science, Toki, Gifu-ken, 509-5292 Japan
2) The Graduate University for Advanced Studies, SOKENDAI, Kanagawa-ken 240-0193, Japan
3) Japan Atomic Energy Agency, Naka, Ibaraki-ken, 311-0193 Japan

email address of main author: hyamada@LHD.nifs.ac.jp

Abstract. High densities exceeding the Greenwald limit by a factor of 1.7 have been obtained in L-mode discharges with high internal inductances of ℓ_i as high as 2.8 in JT-60U. The internal inductance is controlled by ramping down the plasma current. In addition to the extension of the operational regime limited by disruptions, confinement performance remains as good as an H89PL factor of 1.6 even above the Greenwald limit. While an earlier high ℓ_i study has indicated core confinement improvement due to enhancement of the poloidal field, the additional improvement of the tolerance against the high density turned out to be correlated with high edge temperature. The normalized density when the detachment occurs, characterized by a decrease in the Ḍα signal at the divertor**,** is even higher in the case with no disruption than in the case with a disruption. These comparisons have indicated that the improvement in thermal and particle transport does exist in the periphery and in the edge in high ℓ_i plasmas, and the shift of the density limit towards higher densities is observed coincidently. Although the high ℓ_i discharge studied here lies outside of the usual parameter space for steady-state operation of a tokamak, demonstration of a stable discharge with good confinement beyond the Greenwald limit suggests that the magnetic shear at the edge is one key parameter to uncover the physical element**s** of the operational density limit..

1. Introduction

The density limit of magnetically confined plasmas is a critical issue from the perspective of the development of a scenario towards attractive reactors as well as from the view point of the equilibrium limit of a dynamical system. Many experimental works have been dedicated to this issue and consequently the empirical understanding~~s~~ has progressed [1]. In particular, the Greenwald limit which scales only with the product of the plasma current density and elongation [2] has been widely accepted as a reference of the operational density limit in tokamaks. Nonetheless, this phenomenological characteristic is quite empirical and the underlying physics of the Greenwald limit remains an open question. In addition to the operational density limit determined by the occurrence of disruptions [3] or MARFE [4,5,6],

it has been widely recognized that the performance of plasma confinement degrades below the operational density limit [7]. Physics models to describe the core plasma have progressed and simulations based on these advanced models are becoming able to reliably predict future device like ITER. Since the description of edge plasma provides the boundary condition in the simulation of core plasmas, establishment of a model of the edge plasma is prerequisite to predict the global behavior of the plasma. It is plausible that the edge density rather than the core density plays a deterministic role in the density limit [8] since many reports have shown that the peaked density profile in discharges with pellet injection [9,10] or efficient edge pumping [11] allow the higher averaged density operation. Mechanisms leading to edge cooling are often discussed in theoretical approaches to clarify the density limit

In contrast to tokamaks, the operational density regime in stellarators/heliotrons is not limited by disruption but by radiation collapse [12-14]. Therefore power balance and transport play more essential role**s** in the density limit in stellarators/heliotrons than in tokamaks. However, tokamak**s** and stellarators/heliotrons have a wide range of commonality as toroidal system**s** and also the role of plasma currents is supposed to be of much less importance in the edge region because the current itself as well as the current gradient are tiny there. A recent study in LHD suggests that the density where the edge electron temperature falls down to 100 eV is an index of the density limit [11]. Therefore, if confinement (or stability) improvement leading to a higher edge temperature is realized, the density limit in tokamak**s** may be improved as well, in particular, in L mode where the MHD stability limit plays a less deterministic role in characterizing the edge plasma parameter**s** than in H mode.

In this study, we focus on the high ℓ_i L-mode discharges. An earlier work has indicated confinement is improved by an increase in ℓ_i [16,17,18] and its mechanism is attributed to the large poloidal flux or field in the core region. These studies, however, have not explored the density limit and the effect on edge plasmas. The high ℓ_i plasmas are generated transiently by current ramp down and the magnetic shear in the edge region is strengthened simultaneously.

The magnetic shear can stabilize~~d~~ pressure driven modes both in tokamaks and stellarators/heliotrons and also confinement improvement through stabilization of these MHD modes is anticipated. Since it can be postulated that density limit is attributed to the stability itself or instabilities driving transport in the peripheral region, magnetic shear is supposed to affect the density limit.

2. Current Ramp-down Experiment in JT-60U

By making use of the later phase of discharges in JT-60U, ℓ_i and the magnetic shear have been controlled by changing the current ramp down rate (0.175MA/s - 0.75MA/s) from the flat top (I_p=1MA). The region of incidence of disruption has been surveyed together with simultaneous density control. The major and minor radii are 3.4 m and 0.85 m, respectively. The magnetic field ranges between 1.7 and 3.6 T. The change of magnetic field is supposed not to make a difference since the Greenwald density does not depend on the magnetic field. It should be noted that the plasmas studied here are L mode.

Figure 1 shows the waveforms of a discharge with a current ramp down. The plasma current is ramped down from 1MA with the rate of 0.35MA/s. The magnetic field and deposited NBI heating power are 2.1 T and 3.5 MW, respectively. During the ramp down phase, the density is controlled by feedback control. The plasma did not disrupt even in $\bar{n}_e > n_{GW}$, where $n_{GW} = I_p / \pi a^2$ (a represents the horizontal minor radius of the plasma) and the line averaged density $\bar{n}_e$ measured by a tangential CO_2 laser interferometer reached 1.73 times the Greenwald density at t = 11.75 s. While the line averaged density normalized by the Greenwald density, i.e., . $\bar{n}_e / n_{GW}$ is 1.73 well beyond 1, confinement performance is kept as good as H_{89PL} and HH_{y2} factors of 1.6 and 0.99, respectively. These parameters have never been obtained in a flat top phase in JT-60U. Internal inductance ℓ_i reaches 2.84, which suggests a peaked current profile with enhanced magnetic shear. Even in such a high ℓ_i regime, the plasma position is well controlled within ~1 cm for both horizontal axis and vertical axis. Thermal quench indicated by the rapid decay of the stored energy starts at t = 12.02 s when the plasma current I_p is 380 kA. Prior to the thermal quench, contrasting behavior is observed in the outer and inner divertor Dα signals. As the plasma approaches the density limit, both Dα signals rise, which suggests the edge cooling. Then the Dα signal on the inner divertor drops before the Dα signal on the outer divertor since the inner divertor detaches before the outer divertor. The plasma becomes completely detached with the later drop of the Dα signal on the outer divertor.

In a scheme of monotonic current ramp down, magnetic shear and q have colinearity as shown in Fig.2. Here the magnetic shear is defined by $r/q \cdot \mathrm{d}q/\mathrm{d}r$. In order to separate these two factors, the current ramp down is suspended at I_p = 0.65 MA and the phase with decreasing magnetic shear at the constant q is investigated. Figure 3 shows waveforms of this type of discharge. The ℓ_i increases in the current ramp down phase and the density exceeds the Greenwald density. Then ℓ_i starts to decrease in the constant current phase. Correlation of confinement enhancement factor H89PL and ℓ_i is observed clearly. The density also decreases during the constant current phase, although the gas-puffing rate is increased from 17 Pa m^3/s at t=11.0 s to 45 Pa m^3/s at t=11.5 s by a feedback control system to keep the

density constant. The particle confinement degrades with decreasing ℓ_i as well as the energy confinement time. During the steady current phase at I_p=0.65 MA, disruption occurs at even lower normalized density (t=11.8 s). At the pause of the current ramp down at t=11.0 s, the normalized density is 1.41 and ℓ_i is 1.60, while the normalized density and ℓ_i are 1.23 and 1.22 at t=11.75 s, respectively.

Discharges with different ramp down rates and with/without the ramp down pause have been devoted to this kind of experimental sequence. Figure 4 shows the operational density as a function of the Greenwald density. The envelope of the operational density can be described by the Greenwald density for the wide plasma confinement regimes such as L/H-mode, weak positive shear and reversed shear plasmas, where ℓ_i is smaller than 1.1 in the range of $\bar{n}_e / n_{GW} > 0.8$ in JT-60U and does not depend on heating power. However, the high ℓ_i discharges studied here clearly exceed the Greenwald density and provide a new operational regime. The single point well beyond the Greenwald density shown by a triangle is a reversed shear discharge with a density ITB. The edge density is suppressed to 40 % of the Greenwald density in this case [19].

As seen in two discharges illustrated in Fig.1 and 3, the plasma with high ℓ_i extends the operational density regime**,** which is not accessible in regular operation. Figure 5 (a) shows the discharge trajectory on the plane of the internal inductance ℓ_i which is a reference of the strength of the magnetic shear as well**,** and the density normalized by the Greenwald density. Observed trajectories indicate that plasma can enter the high density regime beyond the Greenwald density without disruption with increasing ℓ_i**.** Circles indicate the occurrence of a disruption. The trend that higher density can be obtained with larger ℓ_i, i.e., stronger magnetic shear can be seen. The ratio of radiation from the main chamber P_{rad}^{main} to the NBI heating power P_{NBI} is plotted for the same discharges (see Fig.5(b)). In the investigated discharges, the radiation power is suppressed, which suggests that the role of impurity is not significant in this study.

It is important that this extension of operational density is accompanied by the confinement improvement. Figure 6 shows the confinement enhancement factor on the L mode scaling as a function of ℓ_i. This observation is consistent with an earlier study on high ℓ_i discharges [7] even though the density regime is extended even beyond the Greenwald limit.

3. Characterization of High Internal Inductance Discharges

To clarify the effect of the current ramp-down, characteristics of two discharges are compared

(see Fig.7). One is the discharge shown in Fig.1 and another is the discharge with a slight increase of density and stronger magnetic field (2.5T) than that in the discharge shown in Fig.1 (2.1T). Other operational conditions are arranged in the same. Since the picture of the Greenwald density limit does not depend on the magnetic field, it is plausible that the difference in the magnetic field strength does not make a difference. Increase in the density resulted in the disruption at larger plasma current. Thermal quench starts at I_p of 530 kA in the case with higher density while it starts at I_p of 380 kA in the case with lower density. In the case with higher density, ℓ_i is slightly lower than in the case with lower density.

A characteristic difference in the edge in these two discharges is also observed in the Dα signals from the divertor. Figure 7 (c) and (d) show the extended waveforms of the inner and outer Dα signals at the divertor. The asymmetry in the inner and outer Dα signals, that is the increase in the inner side and the decrease in the outer side, starts at 11.23 s and 11.67 s for the cases with higher and lower densities, respectively. Complete detachment, which is characterized by the abrupt drop of Dα signals on the both sides, occurs at 11.37 s and 11.77 s. Both events are delayed by the higher ℓ_i. The normalized density at the asymmetry of the divertor Dα signal increases from 1.41 to 1.61 with the increase of ℓ_i from 1.88 to 2.56. Also the normalized density at the complete detachment increases from 1.49 to 1.73 with an increase of ℓ_i from 2.06 to 2.95.

Figure 8 shows the profiles of the electron density, electron temperature, q and magnetic shear in these two discharges. The q profile is evaluated from the MSE measurement and the then magnetic shear $r/q \cdot dq/dr$ is derived from the q profile. In the higher density operation (shown in red in Fig.7), the thermal quench starts t = 11.4 s. The profiles in this case are take at t = 11.3s which is 0.1 s prior to the thermal quench and shown by t_e in Fig.7. Hereafter this case is called the earlier disruption. For comparison, the time slice with the same surface q value, i.e., t =11.5 s is taken in the lower density operation (shown in blue in Fig.7). Since the magnetic field is lower, the plasma current to give the same q is lower (483kA). This time slice is shown by t_l in Fig.7 and called the later disruption for convenience. As seen in Fig.8 (a), normalized density of the case with the later disruption is even higher than the case with the earlier disruption. It should be also noted that the case of earlier disruption reaches the density limit while the case of later disruption could have still margin to the density limit. The temperature is higher in the case with the later disruption than the case with the earlier disruption. The case with the earlier disruption has lower ℓ_i (1.94 from the equilibrium calculation and 1.81 from the MSE measurement) than the case with later disruption (2.28 and 1.99 from each evaluation). Although the surface q values are the same, the q profile in the case with later disruption is located below that in the case with the earlier disruption, which

leads to enhanced magnetic shear in the edge. These observations postulate coincidence of magnetic shear and confinement improvement indicated by higher temperature which is favorable to raising the density limit. As seen in Fig.8 (d), the present experimental analysis of the magnetic shear does not quantified the enhancement of the magnetic shear sufficiently, however, it does not contradict this hypothesis.

Figure 9 is the magnetic fluctuation and the divertor Dα signal at the event of complete detachment in the discharge similar to the discharge shown in red in Fig.8. The complete detachment starts around 12.024 s and subsequently a major disruption occurs at 12.051 s. The asymmetry in the Dα signal from the inner and outer divertor appears 0.1 s before the complete detachment although it is out of the frame of Fig.9. Prior to the major disruption, the m/n=2/1 mode with a frequency of 2 kHz was observed in the magnetic probe signals in conjunction with the thermal quench phase. This frequency is consistent with the toroidal rotation velocity, which is measured by the charge exchange-recombination spectroscopy, near the q=2 surface. This observation is consistent with a disruption being triggered by a tearing mode. However, these MHD modes do not appear before the thermal quench and appears after the start of the complete detachment, therefore, they are not the cause but the consequence of the present density limit. The stability analysis of a tearing mode based on a reduced MHD code using cylindrical geometry indicates that linear growth rate and saturated island width are almost the same for both q profiles shown in Fig. 8. The observed difference in q profile does not make a significant difference in stability. The analysis also shows that the tearing mode is destabilized when the current density is largely reduced in the region of r/a>0.6. The observed tearing mode could be destabilized due to complete detachment and following shrinkage of the plasma current channel.

Next is a comparison of the two time slices at t=11.00 s and 11.75 s in the discharge illustrated in Fig.3. This comparison highlights the effect of the magnetic shear since the plasma current is kept constant. Figure 10 shows the electron density, electron temperature, q and the magnetic shear profiles at the end of the current ramp down (t=11.0 s) which gives the maximum ℓ_i and at a time 0.05 s prior to the thermal quench (t=11.75 s). The density normalized by the Greenwald density at each time slice is 1.41 at t=11.0 s and 1.23 at t=11.75s, respectively. During this time frame, ℓ_i decreases from 1.60 to 1.22, which are evaluated by the equilibrium calculation. The estimate from the MSE measurement also indicates the decrease from 1.80 to 1.56. At t=11.0 s, even the density in the peripheral region is higher than at t=11.75 (see Fig.10(a)). The temperature decrease is pronounced in the edge region (see Fig.10(b)). The radiation power increases from 0.75 MW to 1.05 MW, however, this increase is not significant compared with the NBI heating power of 3.2 MW.

Corresponding to the difference in ℓ_i, the MSE measurement suggests that the magnetic shear for $r/a > 0.9$ is stronger at $t = 11.0$ s than at $t = 11.75$ s within the error bars while the surface q is the same because of the same plasma current.

4. Effect of Heating Power on Density Limit

While many studies on the effect of heating power on the density limit suggest that the density limit does not depend on or is not sensitive to the heating power [20], there is some experimental evidence which indicates the heating power dependence on the density limit [21]. Therefore the present study suggests the improvement of the edge electron temperature in high ℓ_i discharges and indicates the effect of heating power on the edge temperature in these discharges. Two discharges with different heating power are compared. In both discharges, the plasma current is ramped down from 1 MA to 0.65 MA with the rate of 0.7 MA/s. Waveforms are illustrated in Fig.11 (a) and (b). In the case of lower heating power (P_{NBI}=4 MW), a disruption occurrs at the density of $0.77n_{GW}$ with an ℓ_i of 1.3 just before the end of the I_p ramp down. In contrast, the discharge with larger heating power (P_{NBI}=10MW) survives for about 1 s after the end of the I_p ramp down and disrupts at 1.0 n_{GW} with ℓ_i of 1.4 during the constant I_p phase of 0.65 MA. The reason why the disruption occurrs in a relatively low density regime compared with discharges shown in Fig.1 and Fig.3 can be attributed to the contamination by Ar which was used in the preceding unfavorable wall condition in these experimental sequences. However the comparison of these two discharges with different heating power is valid because they have the same conditions except for the heating power.

Although the main plasma radiation is larger for the case with higher heating power than the case with lower heating power, the edge electron temperature at r/a =0.94 is kept higher in the case with higher heating power. It is pointed out that the edge electron temperature at the disruption is the same in both discharges. A critical temperature is shown in a band in Fig.11. It should be noted that ℓ_i is almost the same during current ramp-down for these two discharges. This suggests the important element for the density limit is the edge temperature rather than ℓ_i itself. These results support the hypothesis that a large magnetic shear due to high ℓ_i provides confinement improvement and the consequent high edge temperature mitigates the density limit.

5. Summary

L-mode plasmas with high internal inductance ℓ_i have been investigated in terms of the

density limit on JT-60U. During the current ramp down to enhance ℓ_i, it has been found that the density limit with respect the Greenwald limit is significantly raised. In addition to the extension of the operational regime limited by disruptions, confinement performance remains as good as an H89PL factor of 1.~~5~~6 beyond the Greenwald limit by a factor of 1.7. This high performance in the high density regime has not been available in flat top phase in JT-60U. The detachment characterized by the decrease in a Dα signal at the divertor occurs is also shifted to the higher density regime in the discharges with higher ℓ_i. While an earlier study of high ℓ_i for plasmas with moderate density [17] has indicated core confinement improvement due to enhancement of the poloidal field, the high operation is also favorable to raise the density limit. The temperature towards the edge (r/a=0.95) can be kept higher in the discharges with higher ℓ_i. These observations have indicated that the improvement in thermal and particle transport does exist in the periphery and the edge in the high ℓ_i plasmas, which leads to the shift of the density limit towards higher densities. Since ℓ_i is a global zero dimensional parameter, ℓ_i itself is not supposed to be a cause of the improvement of the density limit. These experimental evidences postulate that the enhanced magnetic shear in the edge region due to the current ramp-down is a potential key knob for revealing its physical mechanism. Quantified documentation of the effect of the magnetic shear on the density limit is posed for a future study.

Acknowledgements

This work has been done in the framework of Research Collaboration Using Fusion Research Facilities in JAEA. One of the author (H.Y.) acknowledges the communication with B.J.Peterson.

References

[1] GREENWALD, M., Plasma Phys. Control. Fusion **44** (2002) R27.
[2] GREENWALD, M., et al., Nucl. Fusion **28** (1988) 2199.
[3] ITER EXPERT GROUPS, Nucl. Fusion **39** (1999) 2251.
[4] LIPSCHULTZ, B., et al., Nucl. Fusion **24** (1984) 977.
[5] HOSOGANE, N., et al., J.Nucl. Mater. **196** (1992) 750.
[6] ASAKURA, N., et al., J.Nucl. Mater. **206-209** (1999) 182.
[7] KAMADA, Y., et al., in *Fusion Energy 1996* (Proc.16th Int. Conf. Montreal, 1996) , Vol.1, p.247, IAEA, Vienna (1997).
[8] SUTTROP, W., et al., Plasma Phys. Control. Fusion **39** (1999) 2051.
[9] KAMADA, Y., et al., in *Plasma Physics and Controlled Nuclear Fusion Research 1990* (Proc. 13th Int. Conf. Washington DC, 1990), Vol. 1, p. 291, IAEA,Vienna (1991).
[10] GREENWALD, M., et al., in *Plasma Physics and Controlled Nuclear Fusion Research 1986* (Proc. 11th Int. Conf. Kyoto, 1986), Vol. 1, p. 139, IAEA,

Vienna (1987)
[11] MAINGI, T., et al., J. Nucl. Mater. **266** (1999) 598.
[12] PETERSON, B.J., et al., Phys. Plasmas **8** (2001) 3861.
[13] XU, Y., et al., Nucl. Fusion **42** (2002) 601.
[14] SUDO, S., et al., Nucl. Fusion **30** (1990) 11.
[15] MIYAZAWA, J., et al., in *Fusion Energy 2006* (Proc. 21st Int. Conf. Chengdu, 2006) (Vienna: IAEA) CD-ROM file EX/3-2 and http://www-naweb.iaea.org/napc/physics/FEC/FEC2006/html/index.htm
[16] ZARNSTORFF, M., et al., in *Plasma Physics and Controlled Nuclear Fusion Research 1992* (Proc. 14th Int. Conf. Wuerzburg, 1992), Vol. 1, p. 111, IAEA, Vienna (1993)
[17] KAMADA, Y., et al. Nucl. Fusion **33** (1993) 225.
[18] HOANG, G.T., et al., Nucl. Fusion **34** (1994) 75.
[19] TAKENAGA, H., et al., Nucl. Fusion **45** (2005) 1618.
[20] PETRIE, T.W., et al., Nucl. Fusion **33** (1993) 929.
[21] MERTENS, V., et al., Nucl. Fusion **37** (1997) 1607.

Figure Captions

FIG.1 Discharge with monotonic current ramp down. (a) Plasma current and density. (b) normalized density and internal inductance ℓ_i. (c) Heating and core radiation power. (d) Stored energy and confinement enhancement factor on the ITER-89PL scaling. (e) Dα signals at divertor.

FIG.2 Discharge trajectories on q_{95} and ℓ_i The cases with continuous current ramp-down from 1MA show linear relation between q_{95} and ℓ_i. The pause of the current ramp-down at 0.65MA provides the sequence with changing ℓ_i at constant q_{95}.

FIG.3 Discharge with current ramp down from 1MA and subsequent pause at 0.65MA. (a) Plasma current and density. (b) normalized density and internal inductance ℓ_i. (c) Heating and core radiation power. (d) Stored energy and confinement enhancement factor on the ITER-89PL scaling. (e) Dα signals at divertor. Outer signal is saturated from t=11 s. Profiles at the time slices indicated by t_1(t=10.75s) and t_2(t=11.0s) are discussed in Fig.10

FIG.4 Comparison of experimental density and prediction from scaling of the Greenwald density. The solid line is a reference of $\bar{n}_e^{\exp} = n_e^{GW}$.

FIG.5 (a) Discharge trajectories on ℓ_i and normalized density. (b) Discharge trajectories on normalized density and P_{rad}^{main}/P_{NBI}. Positive spikes seen in the trajectory is due to the breakdown of NBI. For both graphs, solid circles represent the occurrence of a disruption. Trajectories for the solid circles are not shown. Curves are trajectories of typical discharges with current ramp-down in this study. A fat curve is the trajectory of the discharge shown in Fig.1.

FIG.6 Enhancement factor of energy confinement on the L-mode scaling as a function of ℓ_i.The data are evaluated for the discharges plotted in Fig.5

FIG.7 Comparison of extended waveforms of two discharges with earlier/later disruptions. The waveforms shown in red are the same discharge in Fig.1. (a) Plasma current and density normalized by the Greenwald density. (b) Internal inductance ℓ_i. (c) Dα signal at the inner divertor. (d) Dα signal at the outer divertor. The labels of t_e and t_l indicate the time slices of comparison of profiles shown in Fig.8. The dotted vertical lines in (c) and (d) shows the start of asymmetry in Dα signals.

FIG.8 Comparison of profiles at the time slices t_e and t_l in current ramp-down phase of two discharges with earlier/later disruptions shown in Fig.7. (a) Profiles of density normalized by the Greenwald density. (b)Electron temperature profiles. (c) q profiles derived from the MSE measurement. (d) Magnetic shear $r/q \cdot dq/dr$ profiles which are evaluated from the upper and lower envelopes of the q profile including error bars. Errors in the position are not involved in this evaluation.

FIG.9 (a) Fluctuation of poloidal magnetic field and (b) $D\alpha$ signal during detachment leading to a major disruption.

FIG.10 Comparison of profiles at t1 and t2 in the discharge shown in Fig.3. (a) Normalized density profiles.(b) Electron temperature profiles. (c)q profiles derived from the MSE measurement. (d) Magnetic shear $r/q \cdot dq/dr$ profiles which are evaluated from the upper and lower envelopes of the q profile including error bars. Errors in the position are not involved in this evaluation.

FIG.11 Waveforms of current ramp down discharges with the lower NBI heating power of (a) 4MW and (b) 10 MW. From the top to the bottom, plasma current and NBI heating power, line averaged density and the Greenwald density, stored energy and internal inductance, gas flow rate and radiation power in the main chamber, divertor $D\alpha$ signal, and the edge electron temperature are illustrated.

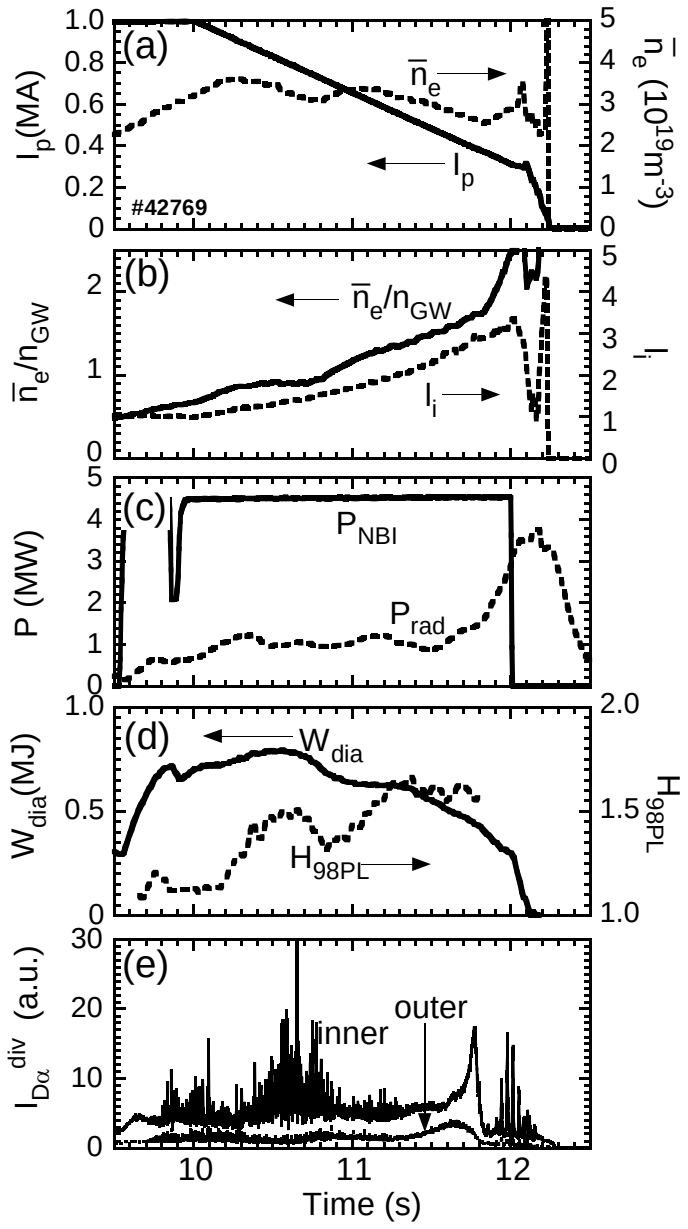

FIG.1 “Density Limit in Discharges with High Internal Inductance on JT-60U” by H.Yamada et al.

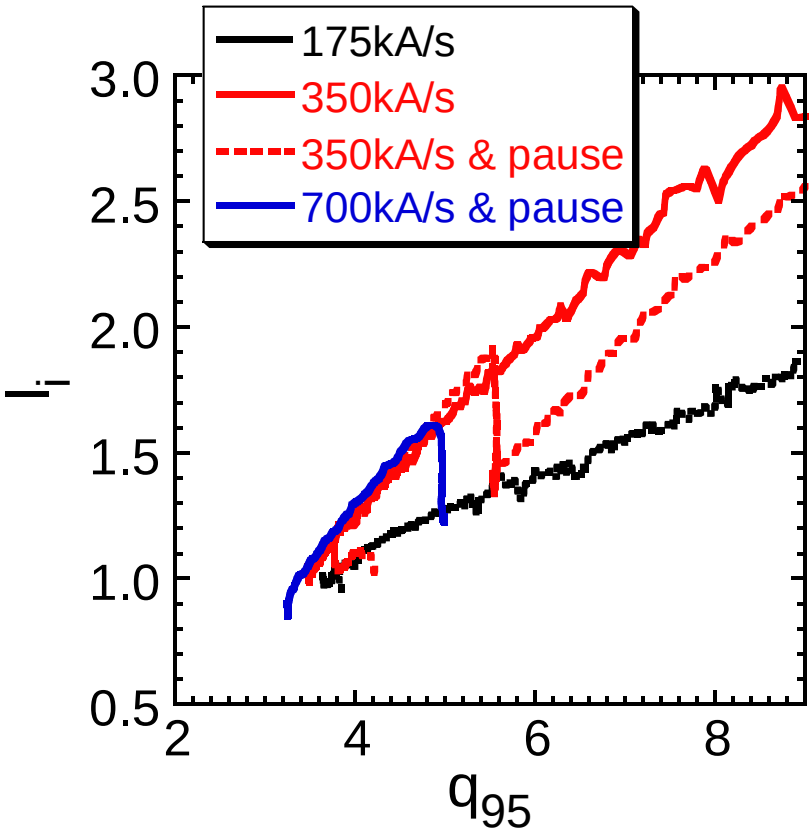

FIG.2 “Density Limit in Discharges with High Internal Inductance on JT-60U” by H.Yamada et al.

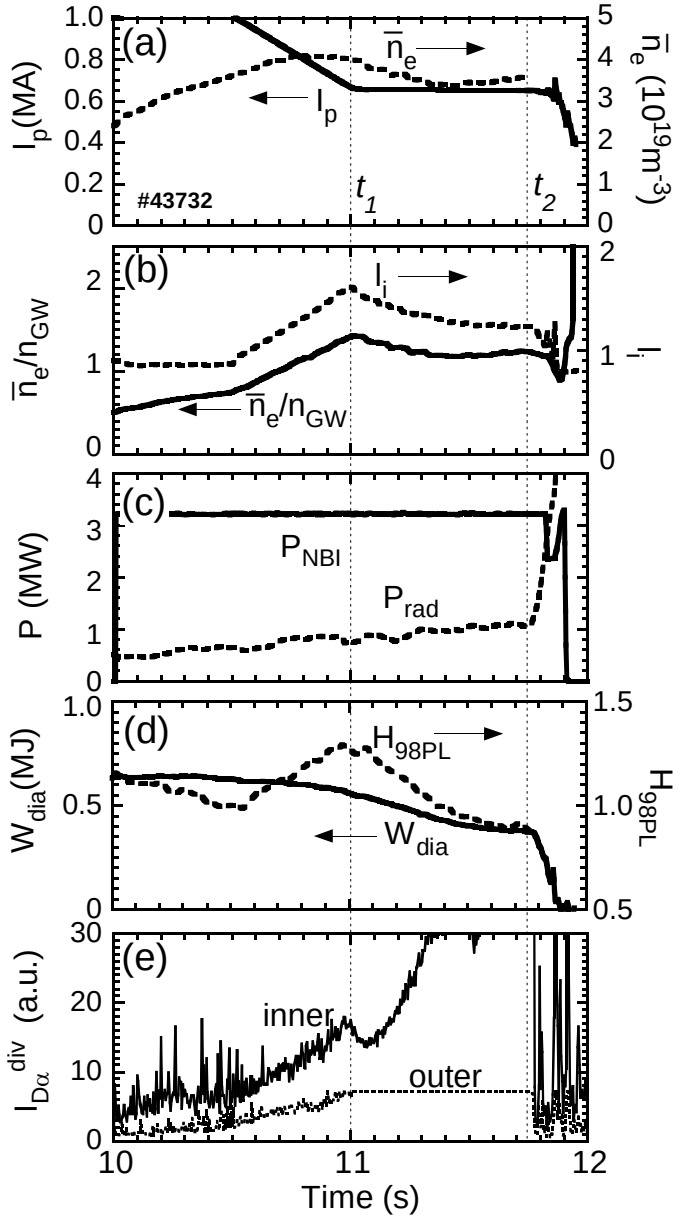

FIG.3 “Density Limit in Discharges with High Internal Inductance on JT-60U” by H.Yamada et al.

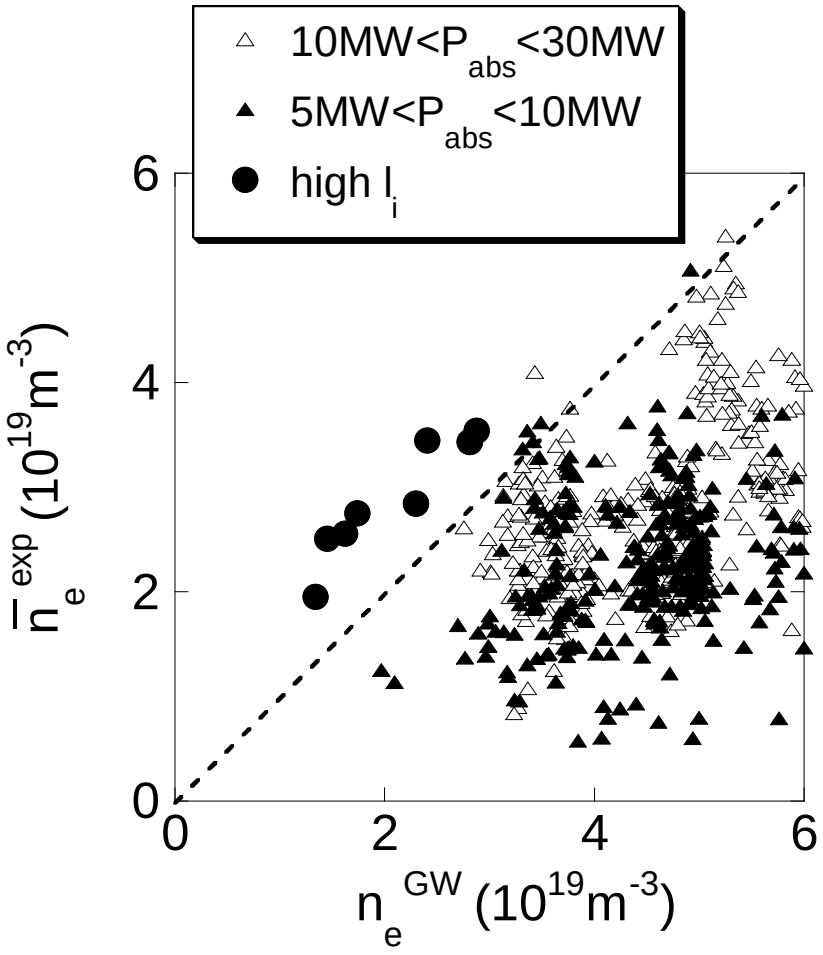

FIG.4 “Density Limit in Discharges with High Internal Inductance on JT-60U” by H.Yamada et al.

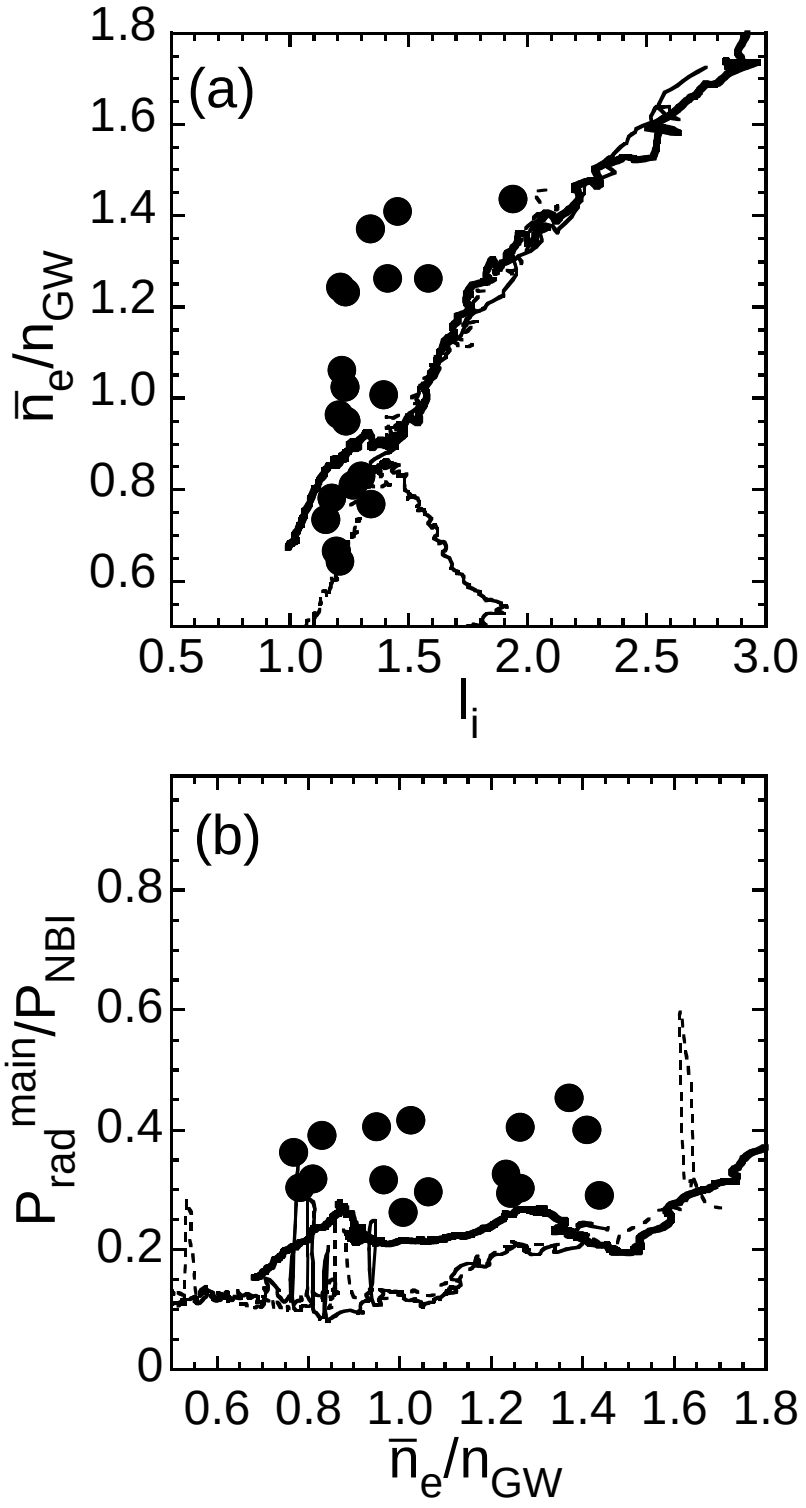

FIG.5 “Density Limit in Discharges with High Internal Inductance on JT-60U” by H.Yamada et al.

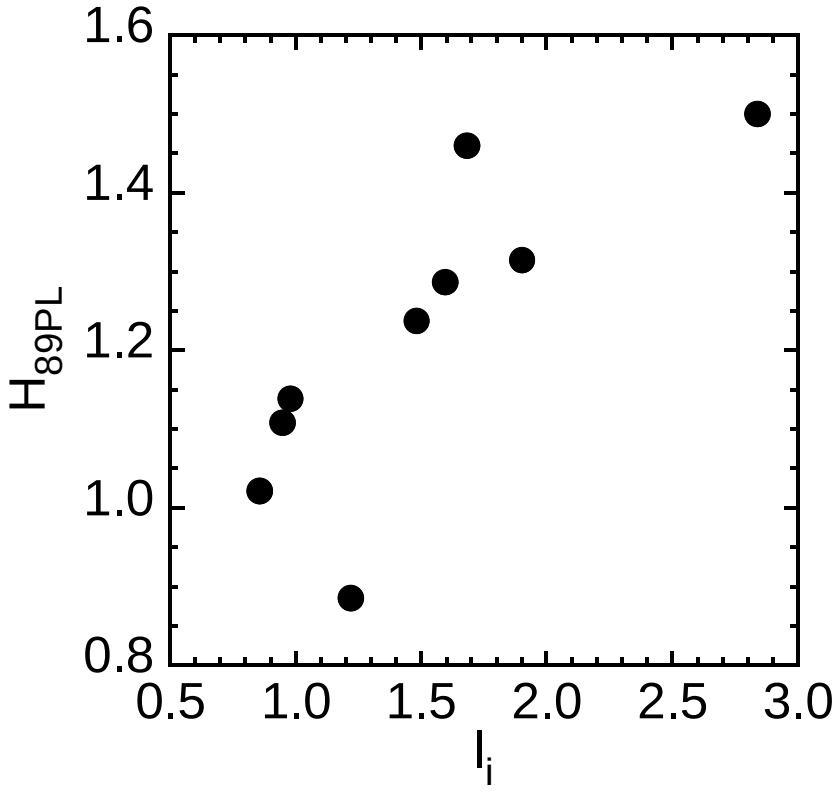

FIG.6 “Density Limit in Discharges with High Internal Inductance on JT-60U” by H.Yamada et al.

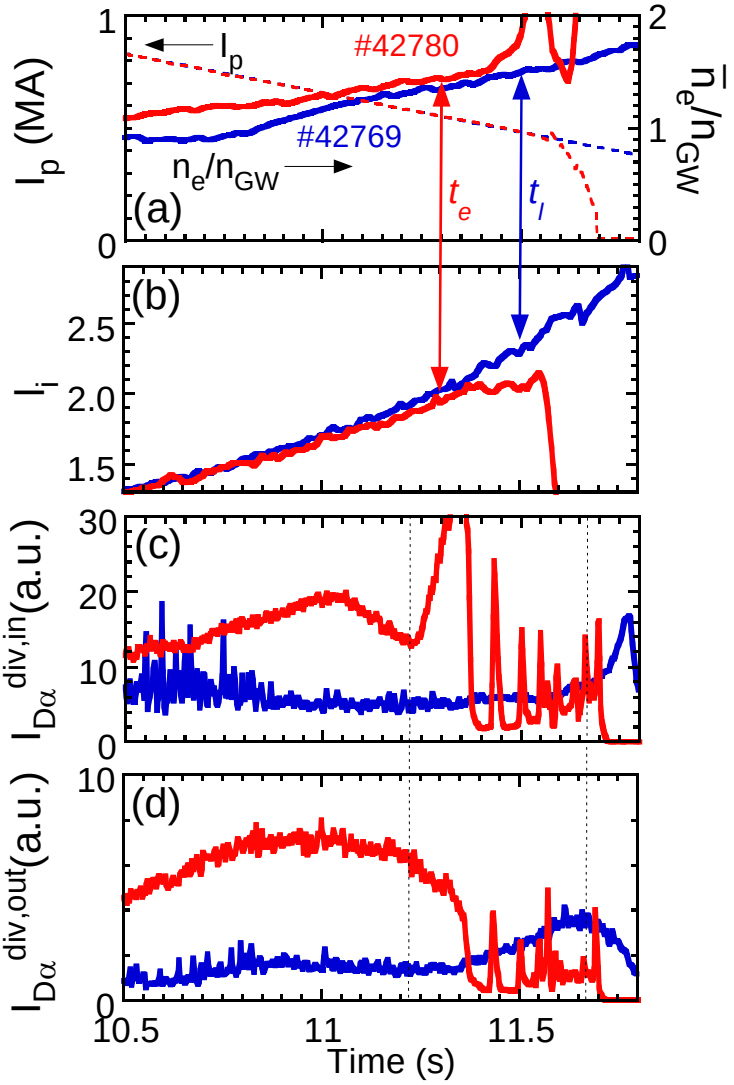

FIG.7 “Density Limit in Discharges with High Internal Inductance on JT-60U” by H.Yamada et al.

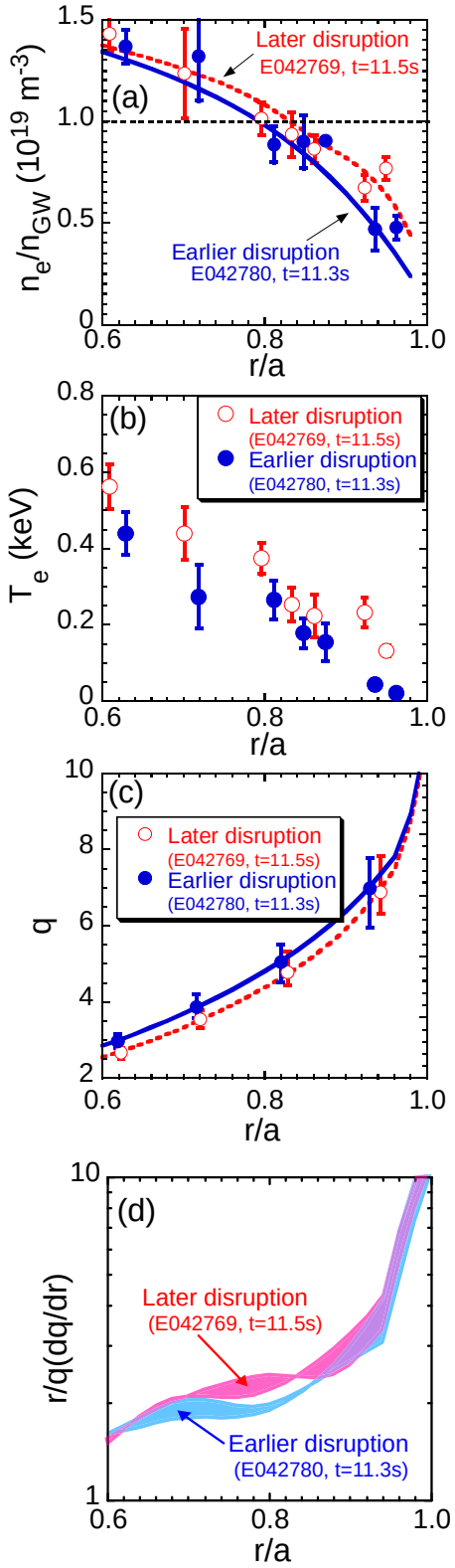

FIG.8 “Density Limit in Discharges with High Internal Inductance on JT-60U” by H.Yamada et al.

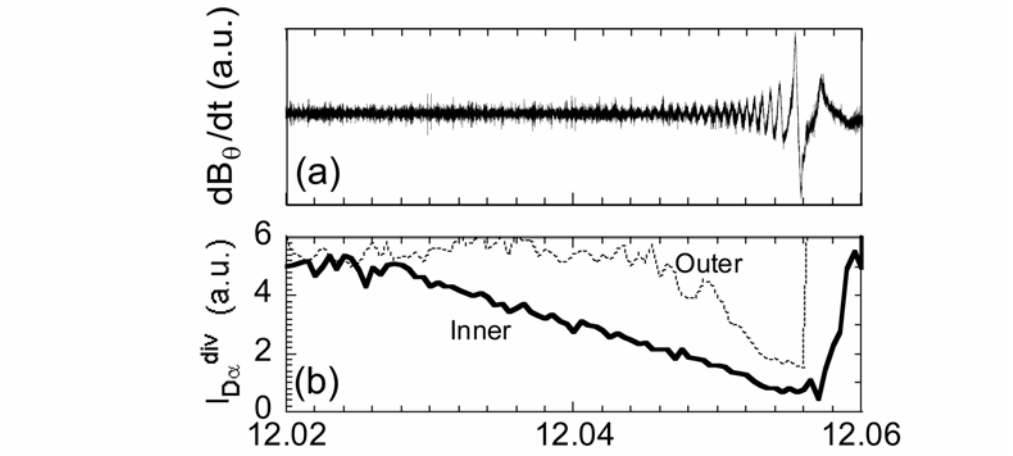

FIG.9 “Density Limit in Discharges with High Internal Inductance on JT-60U” by H.Yamada et al.

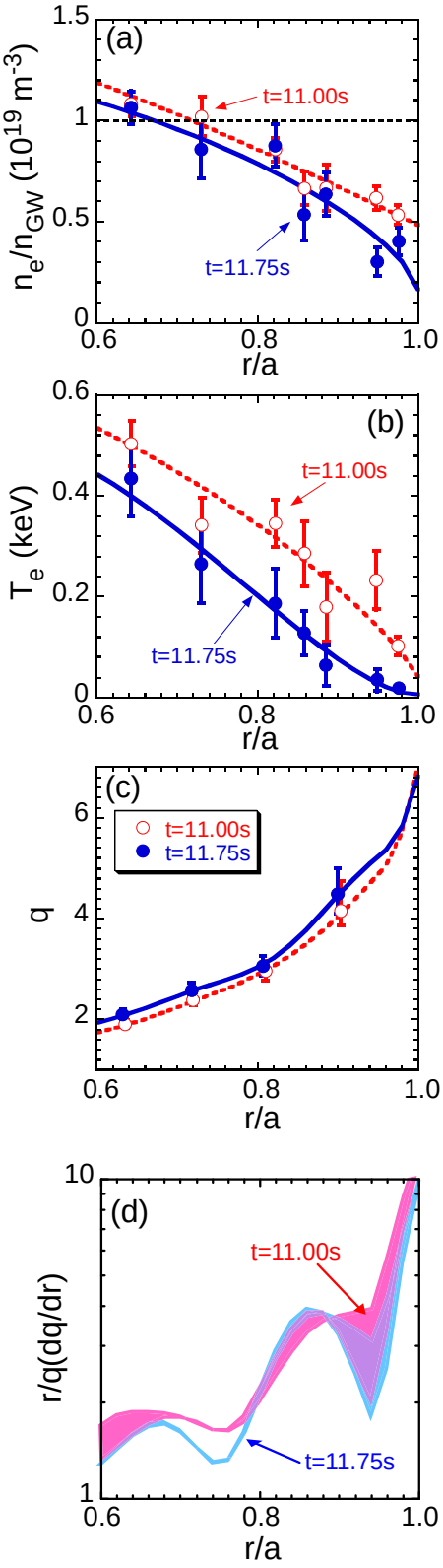

FIG.10 “Density Limit in Discharges with High Internal Inductance on JT-60U” by H.Yamada et al.

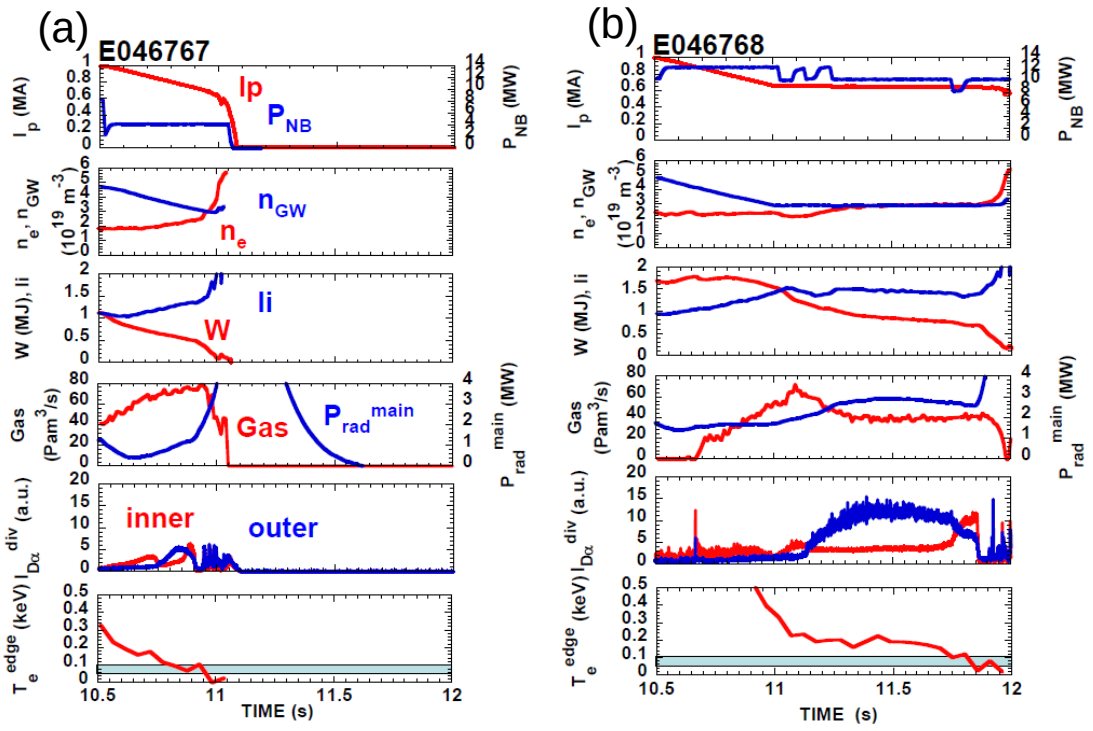

FIG.11 “Density Limit in Discharges with High Internal Inductance on JT-60U” by H.Yamada et al.